## Title
Single-cell resolution of morphological changes in hemogenic endothelium



## Journal
Development, 142(15)

## ISSN
0950-1991

## Authors
Bos, Frank L
Hawkins, John S
Zovein, Ann C

## Publication Date
2015-08-01

## DOI
10.1242/dev.121350

Peer reviewed

© 2015. Published by The Company of Biologists Ltd | Development (2015) 142, 2719-2724 doi:10.1242/dev.121350



# Single-cell resolution of morphological changes in hemogenic endothelium

**Frank L. Bos[1], John S. Hawkins[1] and Ann C. Zovein[1,2,*]**


## ABSTRACT

Endothelial-to-hematopoietic transition (EHT) occurs within a population of hemogenic endothelial cells during embryogenesis, and leads to the formation of the adult hematopoietic system. Currently, the prospective identification of specific endothelial cells that will undergo EHT, and the cellular events enabling this transition, are not known. We set out to define precisely the morphological events of EHT, and to correlate cellular morphology with the expression of the transcription factors RUNX1 and SOX17. A novel strategy was developed to allow for correlation of immunofluorescence data with the ultrastructural resolution of scanning electron microscopy. The approach can identify single endothelial cells undergoing EHT, as identified by the ratio of RUNX1 to SOX17 immunofluorescence levels, and the morphological changes associated with the transition. Furthermore, this work details a new technical resource that is widely applicable for correlative analyses of single cells in their native tissue environments.


**KEY WORDS: Endothelium, Imaging, RUNX1, SOX17, Mice, Human, Hemogenic, Hematopoiesis, Endothelial-to-hematopoietic transition, Scanning electron microscopy**

## INTRODUCTION

Endothelial-to-hematopoietic transition (EHT) during embryogenesis provides the first long-term hematopoietic stem and progenitor cells (HSPC) for the organism. Fate-tracing (Zovein et al., 2008), live-imaging (Bertrand et al., 2010; Boisset et al., 2010; Eilken et al., 2009) and loss-of-function studies (Chen et al., 2009) have demonstrated that a subset of endothelial cells, termed hemogenic endothelium, is capable of generating HSPCs, which first appear as cell clusters of rounded cells attached to the endothelium (North et al., 1999). The best-studied site for HSPC emergence is the developing aorta located in the embryonic aorta-gonad-mesonephros (AGM) region (de Bruijn et al., 2000; North et al., 1999). Intra-aortic hematopoietic clusters appear transiently in the AGM region between embryonic days ~10 and 12 in mouse (de Bruijn et al., 2000) and ~4 and 6 weeks in human (Tavian et al., 1996). *Runx1*, a required transcription factor for the conversion of hemogenic endothelial cells to HSPCs (Chen et al., 2009; North et al., 1999), is first noted within a subset of endothelial cells in hemogenic vascular beds but then localizes to intra-aortic cluster cells (Tober et al., 2013). The transcription factor *Sox17* has also been shown to be important in EHT (Clarke et al., 2013) and hematopoietic stem cell (HSC) survival (Kim et al., 2007). However, whereas *Sox17* promotes hemogenic endothelial specification, continued or overexpression has been noted to inhibit the direct transition to hematopoietic fate (Clarke et al., 2013; Nobuhisa et al., 2014). The relative expression of these two transcription factors (RUNX1 and SOX17) during EHT has not been extensively studied. Here, we present the first report of RUNX1 and SOX17 correlative microscopy analysis in human and murine hemogenic endothelium. The findings illustrate the initiation of EHT on a single-cell level.

[1]Cardiovascular Research Institute, University of California San Francisco, San Francisco, CA 94158, USA. [2]Department of Pediatrics, Division of Neonatology, University of California San Francisco School of Medicine, San Francisco, CA 94143, USA.

*Author for correspondence (ann.zovein@ucsf.edu)

**Received 19 December 2014; Accepted 23 June 2015**

## RESULTS & DISCUSSION

### RUNX1 and SOX17 mark human hemogenic endothelium

We first set out to determine the expression patterns of SOX17 and RUNX1 during human embryonic development. We evaluated the human AGM from 6-8 weeks gestational/menstrual age (GA), which corresponds to developmental stages of 4-6 weeks (Fig. 1; supplementary material Fig. S1). Endothelial cells are identified by PECAM-1 and VE-cadherin (CDH5, referred to here as VEC), whereas CD143 (angiotensin-converting enzyme, ACE) has been shown to identify human AGM endothelium and associated cell clusters (Jokubaitis et al., 2008) (Fig. 1A-E; supplementary material Fig. S1A,B). In addition, as *Runx1* has been demonstrated to be crucial to EHT in the murine system (Chen et al., 2009), we evaluated RUNX1 in human hemogenic endothelial cells and hematopoietic cluster cells (Fig. 1B-G). RUNX1 in the human system is noted within intra-aortic clusters (Fig. 1B,C) but is also present in a small subset of single endothelial cells within the aorta (Fig. 1D-G; supplementary material Fig. S1C,D). In addition, we also observe SOX17 in dorsal aortic endothelial cells (Fig. 1F,G; supplementary material Fig. S1C,D). The localization of SOX17 to arterial endothelium is also observed in another known hemogenic site, the vitelline artery (de Bruijn et al., 2000) (supplementary material Fig. S1E,F). The single endothelial cells within the aorta that exhibit high RUNX1 immunofluorescence also display lower levels of SOX17 immunofluorescence (Fig. 1F,G, arrowheads). As SOX17 and RUNX1 appear to have opposing expression domains, we quantified the levels of RUNX1 and SOX17 per individual aortic endothelial cell, and determined the ratio of RUNX1/SOX17 via mean fluorescence intensities (MFI) of three-dimensional (3D)-rendered nuclear volumes (Fig. 1H-J). Cells with a low ratio (<0.1) are considered mostly endothelial, with near-undetectable levels of RUNX1. High RUNX1/SOX17 ratios (>1) suggest either a hemogenic endothelial cell in transition or hematopoietic cell fate change. Our analysis also reveals endothelial cells that exhibit intermediate ratios, which might represent the early stages of EHT (Fig. 1J). Taken together, during human development, RUNX1 – and, separately, SOX17 – demonstrate high expression in distinct and separate cell populations within the aorta, such that the ratio of RUNX1/SOX17 may predict stages of EHT.

Development (2015) 142, 2719-2724 doi:10.1242/dev.121350

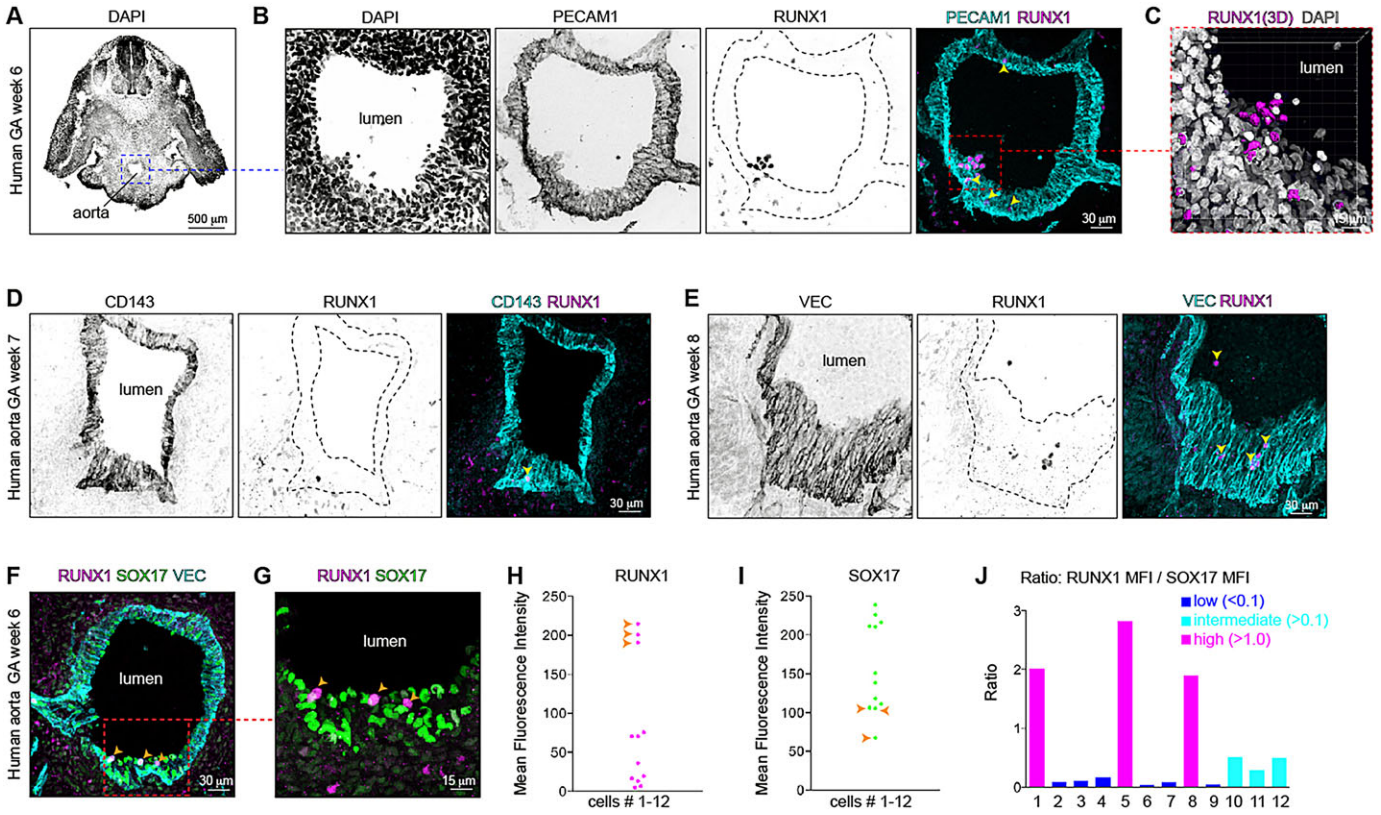


**Fig. 1. Immunofluorescence of human hemogenic endothelium.** (A) GA week 6. DAPI-stained transverse section with dorsal aorta indicated. (B-E) Single channels in black and white. (B) Boxed area in A. PECAM1 (cyan) labels the endothelium and the attached hematopoietic clusters that are also RUNX1$^+$ (magenta). Arrowheads depict single RUNX1$^+$ cells associated with the endothelium. (C) Boxed area in B with DAPI (gray) and 3D volume-rendered RUNX1 (magenta). (D) GA week 7. CD143 (ACE) in cyan labels endothelium and one RUNX1$^+$ (magenta) cell (arrowhead). (E) GA week 8. VEC (CDH5) in cyan labels endothelium, and RUNX1 (magenta) identifies cells in the vascular wall and in circulation (arrowheads). (F) GA week 6. Ventral RUNX1$^+$ (magenta) cells are embedded in VEC$^+$ (cyan) endothelium (arrowheads). SOX17 (green) also labels aortic endothelial cells. (G) Boxed area in F; RUNX1$^+$ (magenta) cells (arrowheads) demonstrate low levels of SOX17 (green). (H,I) Mean fluorescence intensity (MFI) of SOX17 and RUNX1 in selected cells ($n$=12). Arrowheads correspond to values measured in the three cells identified with arrowheads in G. (J) Ratio of RUNX1 MFI to SOX17 MFI of cells in G, and corresponding high (>1.0, magenta), intermediate (>0.1 to <1.0, cyan) and low (<0.1, blue) ratios. The cells indicated with arrowheads in G, and MFIs in H and I, correspond to the high ratios (>1.0) in magenta. (A-G) Scale bars as shown.

### Single-cell analysis of murine hemogenic endothelium reveals hematopoietic transition

In order to study the developmental stages that span hematopoietic emergence, we expanded our evaluation to the murine system. We first investigated hemogenic endothelial sites prior to the appearance of intra-aortic clusters (~E9.5). Endothelial cells exhibited immunofluorescence for VE-cadherin, SOX17 and RUNX1 (Fig. 2; supplementary material Fig. S2A-E). Immunofluorescence levels of RUNX1 and SOX17 with corresponding ratios per individual cell were quantified (Fig. 2A-G). We noted a large range of calculated ratios, possibly representing different stages of EHT (Fig. 2D,F,G). Cells with relatively high ratios could be identified in the aorta (2 out of 60, Fig. 2F) and vitelline artery (2 out of 44, Fig. 2G). We next evaluated intra-aortic clusters, a hallmark of EHT (Fig. 2H-N; supplementary material Fig. S2F-I) at later stages (E10.5-E11.5). Intra-aortic clusters are identified by CD41 (*Itga2b*) (Robin et al., 2011) and *Kit* (referred to here as c-kit) (Yokomizo and Dzierzak, 2010). Using both CD41 and c-kit as markers of hemogenic endothelium and/or EHT, we evaluated RUNX1 and SOX17 within CD41$^+$ and CD41$^-$ populations, as well as within c-kit$^+$ and c-kit$^-$ populations (Fig. 2H-K). Cells identified as c-kit$^+$ or CD41$^+$ consistently exhibited high levels of RUNX1 and low levels of SOX17 (Fig. 2J,K). When both positive and negative populations are evaluated, SOX17 and RUNX1 MFIs exhibit a negative correlation (Fig. 2L). Occasionally we observed a primarily non-nuclear localization of SOX17 in subsets of clusters cells (Fig. 2M), suggesting a possible role for this transcription factor in another cellular compartment. The nuclear ratios of RUNX1/SOX17 per individual cell in a cluster exhibited some variability, but a strong tendency towards ratios >1.0 (18 out of 19), consistent with hematopoietic identity (Fig. 2N). The ratios among endothelial cells near the cluster were notably lower (Fig. 2N), possibly signifying non-hemogenic endothelium.

### Correlative microscopy reveals cellular topography of hemogenic endothelium

To examine the surface morphology of hemogenic endothelium, immunofluorescence was correlated with scanning electron microscopy (SEM) analysis. Images from both types of microscopic evaluation are combined via anatomical landmarks, with a resulting overlay of both immunofluorescence and SEM micrographs. Single cells of entire aortas can be evaluated for RUNX1 and SOX17 with corresponding cellular morphology at ultra-high resolution (Fig. 3; supplementary material Fig. S3). Cells within the hemogenic endothelial layer that exhibit nuclear RUNX1 immunofluorescence are noted to exhibit a range of

Development (2015) 142, 2719-2724 doi:10.1242/dev.121350

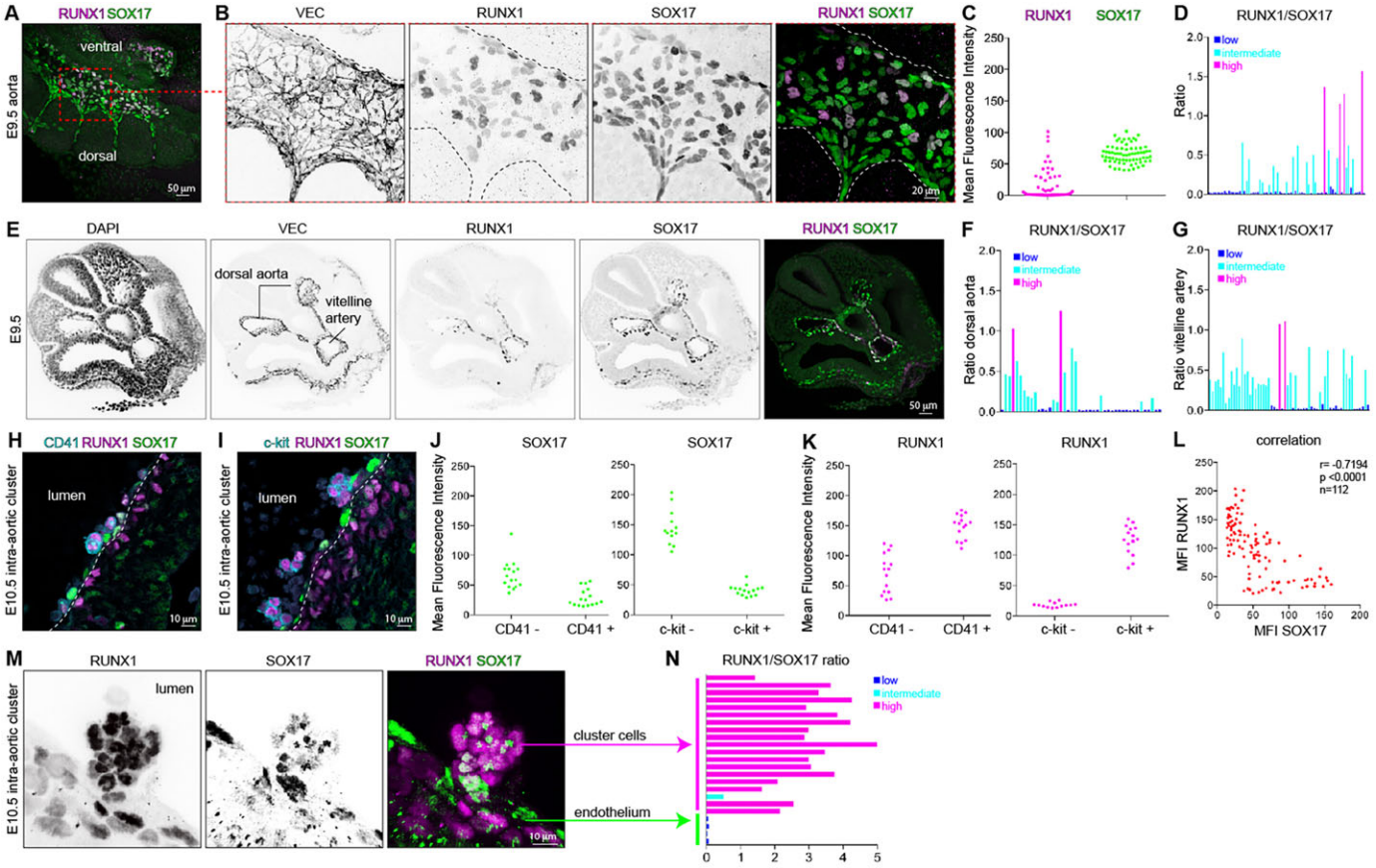


**Fig. 2. RUNX1 and SOX17 in murine hemogenic endothelium.** (A) RUNX1 (magenta) and SOX17 (green) immunofluorescence of E9.5 aorta. (B,E,M) Single channels in black and white. (B) Boxed area in A with single panels of VEC, RUNX1 and SOX17 reveals populations of RUNX1$^+$ (magenta) cells among SOX17$^+$ (green) cells. (C,D) MFI and ratios of RUNX1 and SOX17 per cell pictured in B. High ratios >1.0 (magenta), intermediate (>0.1 to <1.0) in cyan and low ratios (<0.1) in blue. *n*=71. (E) DAPI fluorescence and VEC, RUNX1 (magenta), and SOX17 (green) immunofluorescence in a transverse section of an E9.5 embryo (aorta and vitelline artery as indicated). (F,G) Ratios of RUNX1/SOX17 per single cell in the dorsal aorta (F) and vitelline artery (G) of cells depicted in E reveal ratios >1.0 (magenta bars) in a few cells per anatomical site. *n*=44 and *n*=60, respectively. (H) E10.5 aorta with CD41 (cyan), RUNX1 (magenta) and SOX17 (green). CD41$^+$ marks intra-aortic clusters. (I) E10.5 aorta with c-kit (cyan) and RUNX1 (magenta). SOX17 (green) is noted in the endothelium, whereas RUNX1 is in intra-aortic clusters with membrane expression of c-kit. (J,K) MFI levels of SOX17 (green) and RUNX1 (magenta) in CD41$^+$ and CD41$^-$, and separately in c-kit$^+$ and c-kit$^-$ aortic cells at E10.5. (L) Correlation plot of RUNX1 and SOX17 MFIs of single cells corresponding to image analysis in H-K. Correlation coefficient *r* of −0.78 indicates a strong negative correlation between RUNX1 and SOX17 MFI levels. *P*-value and *n* as shown. (M) RUNX1 (magenta) labels intra-aortic cluster cells with non-nuclear localization of SOX17 (green). (N) RUNX1/SOX17 ratios reveal high (>1.0) ratios in intra-aortic clusters and low ratios (<0.1) in endothelium. (A,B,E,H,I,M) Scale bars as shown.

morphological attributes; as compared with cells that exhibit high SOX17 levels and very low to non-detectable RUNX1 levels (Fig. 3A-D; supplementary material Fig. S3A-H). Overall, the correlative approach defines endothelial cells, with commensurate flat-like cell morphology and integration into the endothelial layer, as exhibiting high SOX17 and low RUNX1 levels (Fig. 3E,F). Strikingly, endothelial cells that exhibit detectable RUNX1 levels demonstrate unique cellular morphology, with more oblong and rounded cell bodies and filopodia-like protrusions of the membrane (Fig. 3E,F; supplementary material Fig. S3I). Thus, the correlative technique allows visualization of aortic endothelium at single-cell resolution with corresponding quantification of immunofluorescence levels and high-resolution cell morphology.

### EHT can be identified through correlative microscopy

In order to identify single hemogenic cells during all stages of EHT, we analyzed complete aortas via our correlative microscopy approach. Murine aortas at E10.5 and E11.5 were analyzed for SOX17 and RUNX1 immunofluorescence and cell surface morphology (Fig. 4; supplementary material Fig. S4), in addition to CD41 and c-kit immunofluorescence (supplementary material Fig. S4A-G). Intra-aortic cluster cells are easily identifiable and exhibit high RUNX1/SOX17 ratios and membrane extensions/protrusions (Fig. 4A-E; supplementary material Fig. S4A-E). We next analyzed single cells embedded within the endothelium. Most cells exhibit high SOX17 levels, but a few cells also exhibit detectable levels of RUNX1 (Fig. 4F,G, magenta and cyan numbers). Overall, our analysis reveals a population of cells with varied RUNX1/SOX17 ratios (Fig. 4H). Cells with little to no RUNX1 exhibit phenotypic endothelial morphology of elongated, flattened cell bodies with smoother cell surfaces (Fig. 4F,G, blue numbers). A higher ratio correlated with rounder morphology and directly correlated with the presence of membrane protrusions (Fig. 4E-G, cyan and pink numbers, Fig. 4I-L; supplementary material Fig. S4H). These protrusions are generally found within the RUNX1$^+$ cell population (Fig. 4I-L). The data demonstrate that as a cell transitions through EHT (as defined by the RUNX1/SOX17 ratio), cell morphological changes occur in association with active changes to the membrane surface.

Development (2015) 142, 2719-2724 doi:10.1242/dev.121350

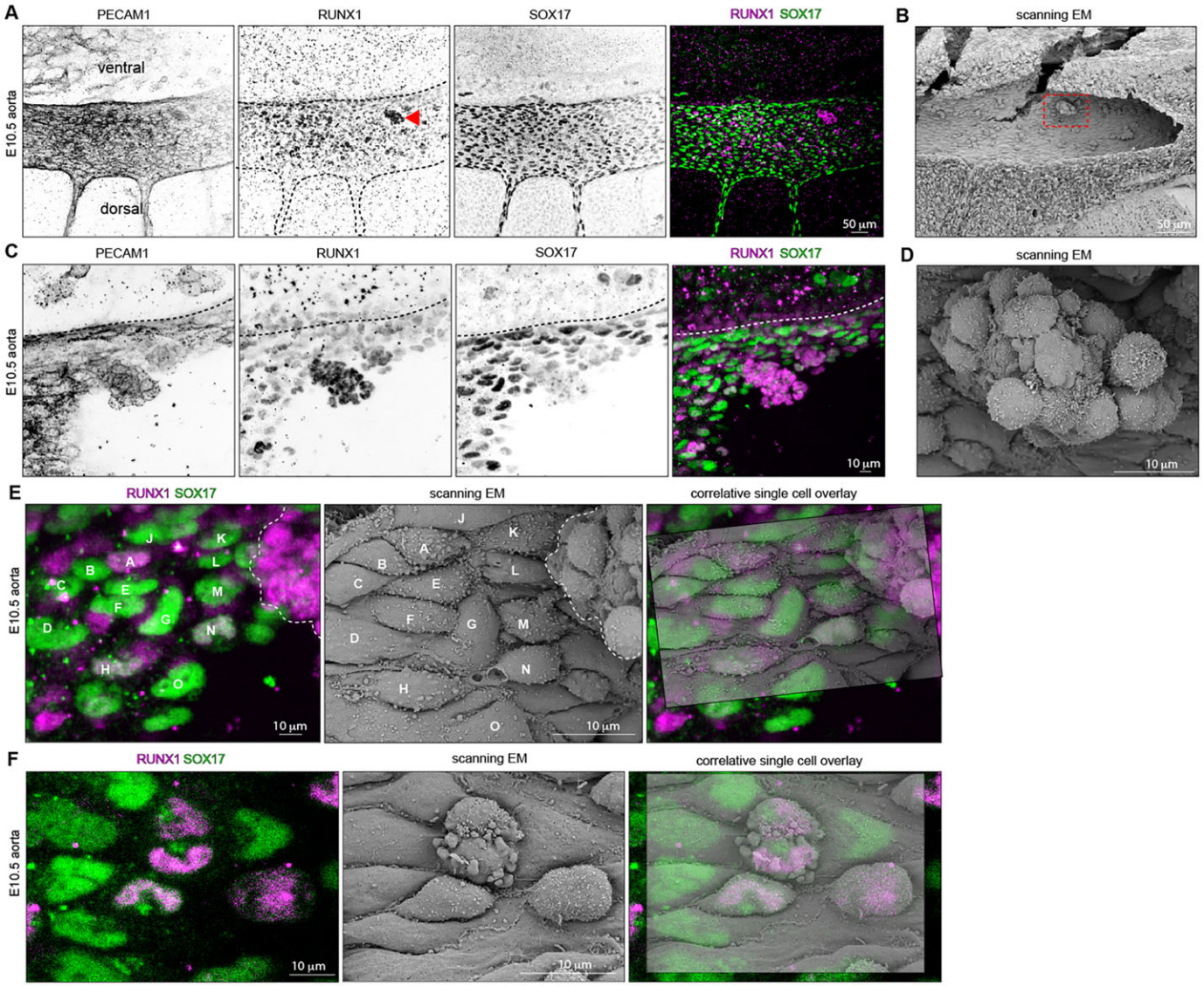


**Fig. 3. Correlative microscopy of aortic endothelium.** (A) E10.5 aorta. RUNX1 (magenta) identifies a large cell cluster (arrowhead), SOX17 in green. Single channels in black and white. (B) Scanning electron micrograph (SEM) of A reveals same cluster (red dashed box). (C) Higher magnification view of large cluster in A marked by PECAM1, RUNX1 (magenta) and SOX17 (green). Single channels in black and white. (D) Scanning EM of boxed region in B demonstrates the heterogeneous membrane morphology of cells comprising the intra-aortic cluster. (E) Endothelium proximal to the large cluster (in B,C and D); cluster identified by the white dashed outline. Each cell is designated by a letter (A-O), with immunofluorescence of SOX17 in green and RUNX1 in magenta, and corresponding scanning EM with overlay. (F) E10.5 aorta with a small group of cells of various cell morphologies and RUNX1 (magenta) and SOX17 (green) immunostaining, with scanning EM and overlay. (A-F) Scale bars as shown.

## Conclusions

By employing the technique of correlative scanning electron microscopy, we have discovered novel cellular events that accompany EHT. Our data demonstrate that during the hemogenic window small perturbations in SOX17 levels are accompanied by increased levels of RUNX1 (which might precede overt morphological changes) and identify a population of hemogenic endothelium. Once RUNX1 levels are increased, with a corresponding decrease in nuclear SOX17, a transition towards hematopoietic fate occurs, as evidenced by rounded cell shape and co-expression of CD41 and/or c-kit (Fig. 4M; supplementary material Fig. S4). In addition, the correlative microscopy approach demonstrates previously uncharacterized changes in membrane dynamics. The significance of membrane protrusions throughout the EHT process is currently unknown. However, similar protrusion-like extensions are observed in immune activation and inflammation (Yamamoto et al., 2015). As inflammation is becoming a more appreciated regulator of HSC emergence (Espín-Palazón et al., 2014; He et al., 2015; Li et al., 2014; Sawamiphak et al., 2014), the observed changes could be due to activation of inflammatory pathways in EHT. Moreover, the observation in the human system that changes in RUNX1 and SOX17 protein levels mirror those seen in the murine system, strongly suggest that similar cellular mechanisms take place in human hemogenic endothelium. These findings and the novel approach will further help to define the changes associated with endothelial-to-hematopoietic conversion. In addition, we introduce a new method of single-cell analysis within tissue/organ and organismal context that is widely applicable to other developmental and cell biological questions.

Development (2015) 142, 2719-2724 doi:10.1242/dev.121350

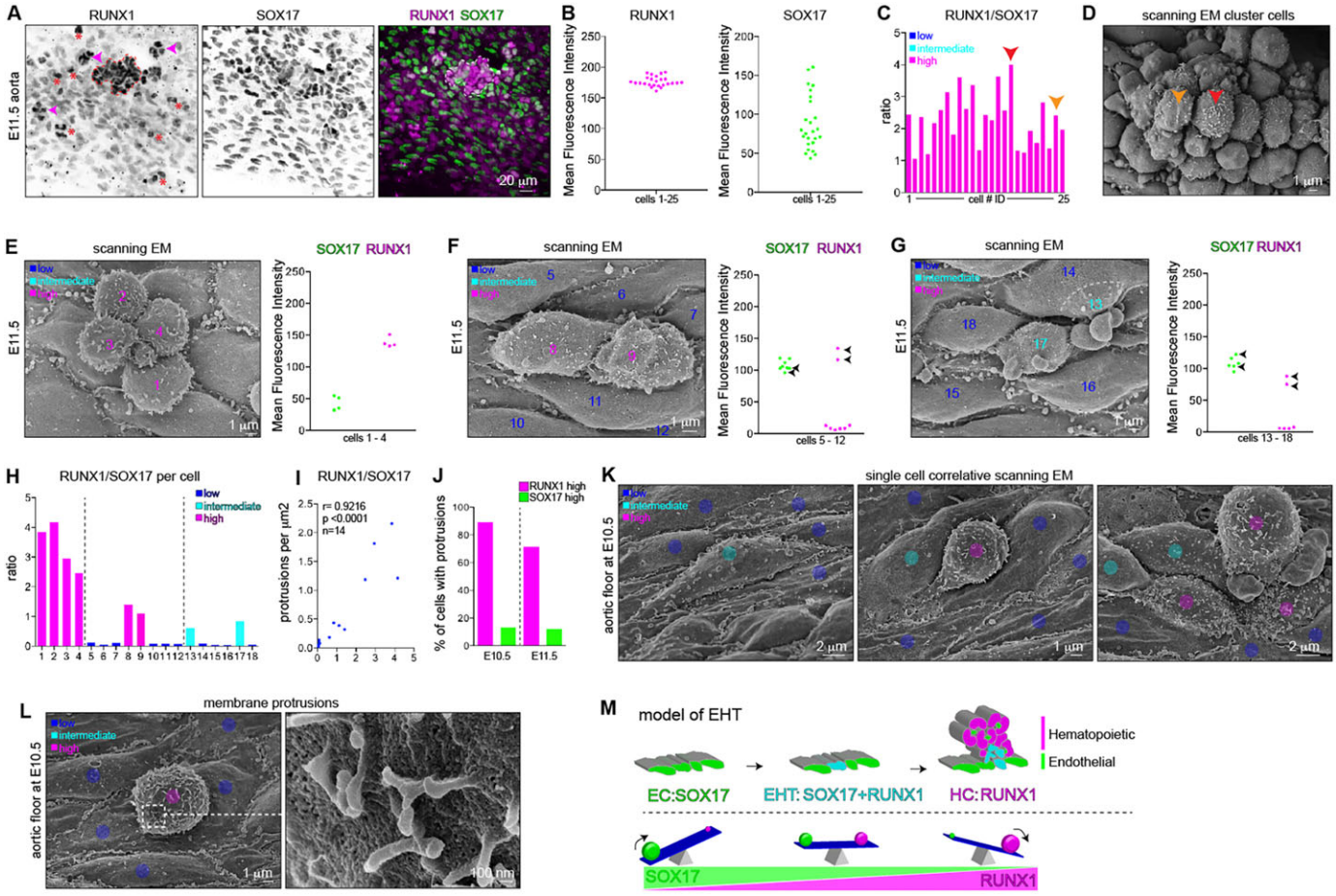


**Fig. 4. Single-cell analysis of endothelial-to-hematopoietic transition.** (A) E11.5 aorta. RUNX1 (magenta) and SOX17 in green. RUNX1$^{+}$ single cells identified by red asterisks, smaller clusters by magenta arrowheads and a large intra-aortic cluster by red dashed outline. Single channels in black and white. (B,C) RUNX1 and SOX17 MFI levels and ratios corresponding to cells in outlined area in A. Red and orange arrows correspond to cells identified in D. *n*=25. (D) SEM image of outlined area in A. The red and orange arrows identify cells with corresponding ratios in C. (E) SEM image of four round cells attached to the endothelium with corresponding high RUNX1 (magenta), low SOX17 (green) MFI levels (right graph). Each cell is numbered in magenta, signifying a high RUNX1/SOX17 ratio per legend. (F) SEM image of cells depicted by colored numbers; colors correspond to ratios per legend. High RUNX1 (magenta) and low-intermediate SOX17 (green) MFI levels of two cells (arrows in right graph) correspond to cells numbered 8 and 9 in magenta. (G) SEM of cells with low and intermediate ratios depicted by colored numbers. RUNX1 and SOX17 MFI levels in right graph; arrows denote two cells with intermediate ratios numbered in cyan (#13 and #17) in left SEM micrograph. Surface morphology does not distinguish cells #13 and #14, but immunofluorescence analysis reveals two nuclei with two different ratios. (H) Bar graph of RUNX1/SOX17 ratios of all numbered cells depicted in E-G separated by dashed lines; colors denote magnitude of ratio per legend, *x*-axis represents the designated cell number. (I) Correlation of RUNX1/SOX17 ratios to number of protrusions per μm$^2$ surface, for cells depicted in E-G. Correlation coefficient *r* suggests a direct correlation of high ratios to more protrusions per cell surface area. *P*-value and *n* as shown. (J) Percentage of cells with protrusions at E10.5 and E11.5 in RUNX1$^{high}$ and SOX17$^{high}$ subpopulations of aortic endothelium. Protrusions can be found primarily in RUNX1$^{high}$ cells. Total number of cells analyzed per aorta at E10.5; RUNX1$^{high}$ (*n*=38), SOX17$^{high}$ (*n*=98). E11.5; RUNX1$^{high}$ (*n*=28), SOX17$^{high}$ (*n*=81). (K) SEM of cells with various ratios denoted by colored dots: high (magenta), intermediate (cyan) and low (blue). (L) Rounded cell with a high ratio (magenta dot), and ultra-high-resolution image (boxed area) of protrusions on the surface of the cell. (M) Schema of the endothelial-to-hematopoietic transition (EHT). EC, endothelial cell; HC, hematopoietic cell. (A,D,E-G,K,L) Scale bars as shown.

## MATERIALS AND METHODS

### Tissue collection

Human tissues were collected in accordance with the regulation and approval of the Committee on Human Research at the University of California, San Francisco, from elective procedures with informed patient consent in strict compliance with legal and ethical regulations. The Carnegie classification system was used for staging and correlated to gestational/menstrual age (GA).

### Animals

Animal protocols were conducted in accordance with University of California at San Francisco Laboratory Animal Research Committee guidelines. Timed pregnancies of wild-type C57Bl/6J animals were dated by vaginal plugs.

### Tissue processing for fluorescent microscopy

Embryos were fixed in 2% paraformaldehyde solution overnight and frozen in Tissue-Tek OCT Compound (Sakura Finetek, 4583). Cryosections of 20-30 μm thickness were obtained (Thermo Scientific Micron, HM550). Slides were dried for 1 h at room temperature (RT), washed with PBST (0.5% Triton-X100) and incubated in blocking buffer (PBST, 5% donkey serum) for 1 h. Primary antibodies (for full list of antibodies please see supplementary material Table S1) were incubated at RT for 6 h in blocking buffer, washed with PBST, incubated with secondary antibody for 1 h, washed, stained with 2 μg/μl DAPI and mounted in Vectamount (Vector Laboratories, H-5501). Images were captured on a Leica SPE Confocal Microscope and/or Zeiss LSM 780 and compiled using ImageJ and Imaris 7.6 (Bitplane) software.

### Tissue processing and correlative microscopy

Embryos were fixed as described above, washed in PBS and embedded in 4% low-melting-point agarose, sectioned on a vibratome (Leica VT 100P) at 100-300 μm. Samples were incubated with 1.0% Triton-X100 in PBS for 1 h, immunostained and imaged as described above. Following image

Development (2015) 142, 2719-2724 doi:10.1242/dev.121350

acquisition, samples were re-fixed in 0.1 M sodium cacodylate/1% glutaraldehyde, pH 7.5, for 1 h, washed in 0.1 M sodium cacodylate, then dehydrated in a series of EtOH (30, 50, 70, 90, 100%) and dried using a critical-point dryer, followed by 8 nm Ir labeling prior to image acquisition on a Zeiss Ultra55 FE-SEM.

### Single-cell analysis

For single-cell analysis images were acquired with optimal *z*-stack distance ranging from 0.5 to 1.0 µm per stack in 8-bit modus. Image files were analyzed using Imaris 7.6 (Bitplane) software. Each individual cell nucleus was volume-rendered based on fluorescence signal from DAPI, SOX17 or RUNX1, using a surface creation algorithm (Imaris 7.6, Bitplane) in order to generate a measurement per channel of fluorescence intensity. Mean fluorescence intensities (MFI) ranged from 0 to a max of 255. For cells with nuclear SOX17 immunofluorescence, MFIs were measured based on volumes rendered via SOX17. RUNX1 3D nuclear rendering was employed when SOX17 was minimally co-localized with DAPI. Protrusions per cell were measured using FIJI software by determining surface area per cell and total protrusions surface area as percentage of total surface coverage area. Correlation coefficient $r$ was determined by computing X versus Y parameters (ratios versus protrusions, and RUNX1 MFI versus SOX17 MFI) via non-parametric Spearman correlation in GraphPad (Prism). Cells visualized having protrusions uniformly covering >10% of their surface area were scored as positive for calculation of percentages.

### Image acquisition and image comparison

Owing to inherent variability between microscopes, staining protocols and developmental stages of the tissue, image files obtained from separate microscopes Zeiss LSM 780 and Leica SPE did not undergo cross-comparative analyses. Only single cells within a single generated image file were compared with each other, but not between image files. Comparisons were measured via MFI of RUNX1 and SOX17. The ratio was determined by dividing the MFI of RUNX1 by SOX17.

#### Acknowledgements

We acknowledge Drs Clive Hayzelden and Diana Mars for their assistance with the Carl Zeiss Ultra 55 FE-SEM core at San Francisco State University.

#### Competing interests

The authors declare no competing or financial interests.

#### Author contributions

F.L.B. and A.C.Z. designed/planned experiments. F.L.B. performed experiments with assistance from J.S.H. F.L.B. and A.C.Z. wrote the manuscript, with contributions from J.S.H.

#### Funding

This work was supported by the NWO Rubicon Award and a Netherlands KWF Fellowship (both to F.L.B.); the Burroughs Wellcome Fund [1008408.01 to A.C.Z.], the National Institutes of Health (NIH) Innovator Award program [DP2-HL117743-01 to A.C.Z.] and the California Institute for Regenerative Medicine [RN3-06479 to A.C.Z.]. FE-SEM and supporting facilities were funded by NSF-MRI #0821619 and NSF-EAR #0949176, respectively. Deposited in PMC for release after 12 months.

#### Supplementary material

Supplementary material available online at
http://dev.biologists.org/lookup/suppl/doi:10.1242/dev.121350/-/DC1

#### References

**Bertrand, J. Y., Chi, N. C., Santoso, B., Teng, S., Stainier, D. Y. R. and Traver, D.** (2010). Haematopoietic stem cells derive directly from aortic endothelium during development. *Nature* **464**, 108-111.

**Boisset, J.-C., van Cappellen, W., Andrieu-Soler, C., Galjart, N., Dzierzak, E. and Robin, C.** (2010). In vivo imaging of haematopoietic cells emerging from the mouse aortic endothelium. *Nature* **464**, 116-120.

**Chen, M. J., Yokomizo, T., Zeigler, B. M., Dzierzak, E. and Speck, N. A.** (2009). Runx1 is required for the endothelial to haematopoietic cell transition but not thereafter. *Nature* **457**, 887-891.

**Clarke, R. L., Yzaguirre, A. D., Yashiro-Ohtani, Y., Bondue, A., Blanpain, C., Pear, W. S., Speck, N. A., Keller, G.** (2013). The expression of Sox17 identifies and regulates haemogenic endothelium. *Nat. Cell Biol.* **15**, 502-510.

**de Bruijn, M. F. T. R., Speck, N. A., Peeters, M. C. E. and Dzierzak, E.** (2000). Definitive hematopoietic stem cells first develop within the major arterial regions of the mouse embryo. *EMBO J.* **19**, 2465-2474.

**Eilken, H. M., Nishikawa, S.-I. and Schroeder, T.** (2009). Continuous single-cell imaging of blood generation from haemogenic endothelium. *Nature* **457**, 896-900.

**Espín-Palazón, R., Stachura, D. L., Campbell, C. A., García-Moreno, D., Del Cid, N., Kim, A. D., Candel, S., Meseguer, J., Mulero, V. and Traver, D.** (2014). Proinflammatory signaling regulates hematopoietic stem cell emergence. *Cell* **159**, 1070-1085.

**He, Q., Zhang, C., Wang, L., Zhang, P., Ma, D., Lv, J. and Liu, F.** (2015). Inflammatory signaling regulates hematopoietic stem and progenitor cell emergence in vertebrates. *Blood* **125**, 1098-1106.

**Jokubaitis, V. J., Sinka, L., Driessen, R., Whitty, G., Haylock, D. N., Bertoncello, I., Smith, I., Péault, B., Tavian, M. and Simmons, P. J.** (2008). Angiotensin-converting enzyme (CD143) marks hematopoietic stem cells in human embryonic, fetal, and adult hematopoietic tissues. *Blood* **111**, 4055-4063.

**Kim, I., Saunders, T. L. and Morrison, S. J.** (2007). Sox17 dependence distinguishes the transcriptional regulation of fetal from adult hematopoietic stem cells. *Cell* **130**, 470-483.

**Li, Y., Esain, V., Teng, L., Xu, J., Kwan, W., Frost, I. M., Yzaguirre, A. D., Cai, X., Cortes, M., Maijenburg, M. W. et al.** (2014). Inflammatory signaling regulates embryonic hematopoietic stem and progenitor cell production. *Genes Dev.* **28**, 2597-2612.

**Nobuhisa, I., Osawa, M., Uemura, M., Kishikawa, Y., Anani, M., Harada, K., Takagi, H., Saito, K., Kanai-Azuma, M., Kanai, Y. et al.** (2014). Sox17-mediated maintenance of fetal intra-aortic hematopoietic cell clusters. *Mol. Cell. Biol.* **34**, 1976-1990.

**North, T., Gu, T. L., Stacy, T., Wang, Q., Howard, L., Binder, M., Marín-Padilla, M. and Speck, N. A.** (1999). Cbfa2 is required for the formation of intra-aortic hematopoietic clusters. *Development* **126**, 2563-2575.

**Robin, C., Ottersbach, K., Boisset, J.-C., Oziemlak, A. and Dzierzak, E.** (2011). CD41 is developmentally regulated and differentially expressed on mouse hematopoietic stem cells. *Blood* **117**, 5088-5091.

**Sawamiphak, S., Kontarakis, Z. and Stainier, D. Y. R.** (2014). Interferon gamma signaling positively regulates hematopoietic stem cell emergence. *Dev. Cell* **31**, 640-653.

**Tavian, M., Coulombel, L., Luton, D., Clemente, H. S., Dieterlen-Lievre, F. and Peault, B.** (1996). Aorta-associated CD34+ hematopoietic cells in the early human embryo. *Blood* **87**, 67-72.

**Tober, J., Yzaguirre, A. D., Piwarzyk, E. and Speck, N. A.** (2013). Distinct temporal requirements for Runx1 in hematopoietic progenitors and stem cells. *Development* **140**, 3765-3776.

**Yamamoto, S., Niida, S., Azuma, E., Yanagibashi, T., Muramatsu, M., Huang, T. T., Sagara, H., Higaki, S., Ikutani, M., Nagai, Y. et al.** (2015). Inflammation-induced endothelial cell-derived extracellular vesicles modulate the cellular status of pericytes. *Sci. Rep.* **5**, 8505.

**Yokomizo, T. and Dzierzak, E.** (2010). Three-dimensional cartography of hematopoietic clusters in the vasculature of whole mouse embryos. *Development* **137**, 3651-3661.

**Zovein, A. C., Hofmann, J. J., Lynch, M., French, W. J., Turlo, K. A., Yang, Y., Becker, M. S., Zanetta, L., Dejana, E., Gasson, J. C. et al.** (2008). Fate tracing reveals the endothelial origin of hematopoietic stem cells. *Cell Stem Cell* **3**, 625-636.